

## PVP-stabilized tungsten oxide nanoparticles (WO<sub>3</sub>) nanoparticles cause hemolysis of human erythrocytes in a dose-dependent manner

A. L. Popov<sup>1</sup>, I. V. Savintseva<sup>1</sup>, N. R. Popova<sup>1</sup>, T. O. Shekunova<sup>2,3</sup>, O. S. Ivanova<sup>3</sup>,  
A. B. Shcherbakov<sup>4</sup>, D. A. Kozlov<sup>2,3</sup>, V. K. Ivanov<sup>2,3\*</sup>

<sup>1</sup>Institute of Theoretical and Experimental Biophysics, Russian Academy of Sciences,  
Pushchino, Moscow region, 142290, Russia

<sup>2</sup>Lomonosov Moscow State University, Moscow, 119991, Russia

<sup>3</sup>Kurnakov Institute of General and Inorganic Chemistry, Russian Academy of Sciences, Moscow, 119991, Russia

<sup>4</sup>Zabolotny Institute of Microbiology and Virology, National Academy of Sciences of Ukraine,  
Kyiv, D0368, Ukraine

antonpopovleonid@gmail.com, savintseva\_irina@mail.ru, nellipopovaran@gmail.com,  
taisia.shekunova@yandex.ru, runetta05@mail.ru, carotene@igic.ras.ru, kozlov@inorg.chem.msu.ru,  
\*van@igic.ras.ru

PACS 68.65.k, 81.20.n, 82.70.Dd, 87.17.Ec

DOI 10.17586/2220-8054-2019-10-2-199-205

Tungsten oxide nanoparticles (WO<sub>3</sub> NPs) are increasingly being considered as a promising material for biomedical applications. However, toxicological information on their effect on red blood cells (RBCs) remains very scarce. In this study, we examined the toxicity of PVP-stabilized tungsten oxide nanoparticles against human RBCs. Optical microscopy and spectrophotometry data showed that WO<sub>3</sub> NPs induce hemolytic activity. This effect is probably attributed to the direct interaction of the nanoparticles with the RBCs, resulting in the oxidative stress, membrane injury, and subsequent hemolysis.

**Keywords:** tungsten oxide nanoparticles, human erythrocytes, hemolysis.

*Received: 10 February 2019*

*Revised: 21 February 2019*

### 1. Introduction

Tungsten oxide nanoparticles (WO<sub>3</sub> NPs) are considered as a promising nanomaterial for biomedical applications due to their multifunctionality and therapeutic importance. In recent years, WO<sub>3</sub> NPs have been employed in advanced biomedical applications as antibacterial coatings, contrast agents for X-ray computed tomography or biosensors [1–8]. However, a comprehensive multi-faceted study of their cytotoxicity, in particular hemotoxicity, is still missing. Meanwhile, hemolytic analysis is mandatory for all types of nanomaterials, since their hemolytic activity depends strongly on the size, shape and charge of the nanoparticles, as well as synthesis approaches. Earlier, Chen et al. examined the size-dependent cytotoxicity of silver nanoparticles (Ag NPs) against fish RBCs using three different preparations with characteristic size of nanoparticles of 15 nm, 50 nm, or 100 nm. Data obtained showed that Ag NPs exhibited size effect on their adsorption and uptake by RBCs: the smaller particles possess higher hemolytic activity than that of the larger particles [9]. Aisaka et al. demonstrated hemoglobin release from human erythrocytes upon incubation with TiO<sub>2</sub> nanoparticles. However, the hemolysis was abolished by plasma, and so physical (mechanical) factors are the most important in TiO<sub>2</sub>-induced hemolysis [10]. Vinardell et al. compared the hemolytic behavior of bulk aluminum oxide and aluminum oxide nanoparticles on erythrocytes from humans, rats and rabbits. Aluminum oxide nanoparticles are less hemolytic than bulk aluminum oxide and aluminum oxide nanowires, and behave differently depending on the size and shape of the particles [11]. Babu et al. investigated the size-dependent interaction of zinc oxide nanoparticles (ZnO NPs) with RBCs, and their impact on cell viability, DNA damage, reactive oxygen species (ROS) generation. Results obtained showed that ZnO NPs exhibited a size dependent effect on RBCs and hemoglobin (Hb), particularly those NPs with size less than 50 nm [12].

Considering WO<sub>3</sub> nanoparticles as a promising contrast agent for X-ray computed tomography, one should analyze their effect on human blood cells. Here, we evaluated the hemolytic activity of PVP-stabilized WO<sub>3</sub> nanoparticles and suggested possible WO<sub>3</sub> nanoparticles cytotoxicity mechanisms.

## 2. Materials and methods

### 2.1. Synthesis and characterization of tungsten oxide nanoparticles (WO<sub>3</sub> NPs)

Ultrasmall hydrated tungsten oxide nanoparticles were synthesized by hydrothermal processing of tungstic acid in the presence of polyvinylpyrrolidone (PVP K-30, average mol. wt. 40,000) as template, stabilizer and growth regulator. Tungstic acid was prepared by ion-exchange method using sodium tungstate (Na<sub>2</sub>WO<sub>4</sub>) solution and strongly acidic cation exchange resin (Amberlite® IR120). Briefly, ion exchange resin (in a hydrogen form) was swelled in water and loaded into the glass column (filling volume 200 ml). Then, 100 ml of 0.05 M sodium tungstate solution was passed through the column dropwise; 4 g of PVP was added to the obtained eluent; solution was transferred to the flask and stirred for 4 h at reflux. During heating a clear sol of hydrated WO<sub>3</sub> was formed, as evidenced by the appearance of UV-absorption band at 325 nm and Tyndall cone. For cell experiments, sol obtained was diluted to prepare 0.1 – 25.0 mg/ml WO<sub>3</sub> colloid solutions.

In order to determine the possible influence of polyvinylpyrrolidone stabilizer (PVP) on RBCs, we also prepared individual PVP solutions in a similar way.

High-resolution transmission electron microscopy (HR-TEM) analysis was performed using a Libra 200 MC microscope (Zeiss, Germany). TEM images were recorded using a CCD camera (Gatan, USA) with a matrix size of 4096 × 4096 pixels.

X-ray diffraction (XRD) patterns were collected using a Rigaku D/MAX 2500 diffractometer (Bragg–Brentano reflection geometry) with a scintillation counter. All measurements were performed with CuK $\alpha_{1,2}$  radiation generated on a rotating Cu anode (50 kV, 250 mA) and monochromatized by a curved graphite [0 0 2] monochromator. XRD patterns were obtained in the 2 $\theta$  range 5 – 80° at a 2 $\theta$  step of 0.02° and a counting time at least of 10 s per step. Before the measurements the WO<sub>3</sub> sols were applied to an ITO substrate and dried.

The FTIR spectra of the samples were recorded on a Bruker ALPHA spectrometer, in a range of 400 – 4000 cm<sup>-1</sup>, in attenuated total reflectance mode. To avoid solvent effect WO<sub>3</sub> sol and PVP solution were dried at 50 °C for 1 h.

### 2.2. Analysis of hemolytic activity

The analysis of hemolytic activity was performed on human blood collected from a healthy patient. The method for hemolysis assay was reported earlier [13]. Prior to WO<sub>3</sub> nanoparticles exposure, the absorbance spectrum of the positive control supernatant was checked and used only when the optical density was in the range of 0.50 – 0.55. Red blood cells (RBCs) were then incubated with WO<sub>3</sub> nanoparticles for 2 h and further centrifuged to isolate the cells. After that, 100  $\mu$ L of supernatant for each sample was transferred to a 96-well plate. The absorbance values of the supernatant at 570 nm were determined by using a microplate reader. The percent hemolysis of RBCs was calculated according to the equation: percent hemolysis = ((sample absorbance – negative control absorbance)/(positive control absorbance – negative control absorbance)) × 100.

### 2.3. Optical microscopy of RBCs

Optical microscopy images of RBCs incubated with WO<sub>3</sub> nanoparticles were taken using a Carl Zeiss Axiovert 200 fluorescence-light microscope and recorded by a Canon A620 digital camera.

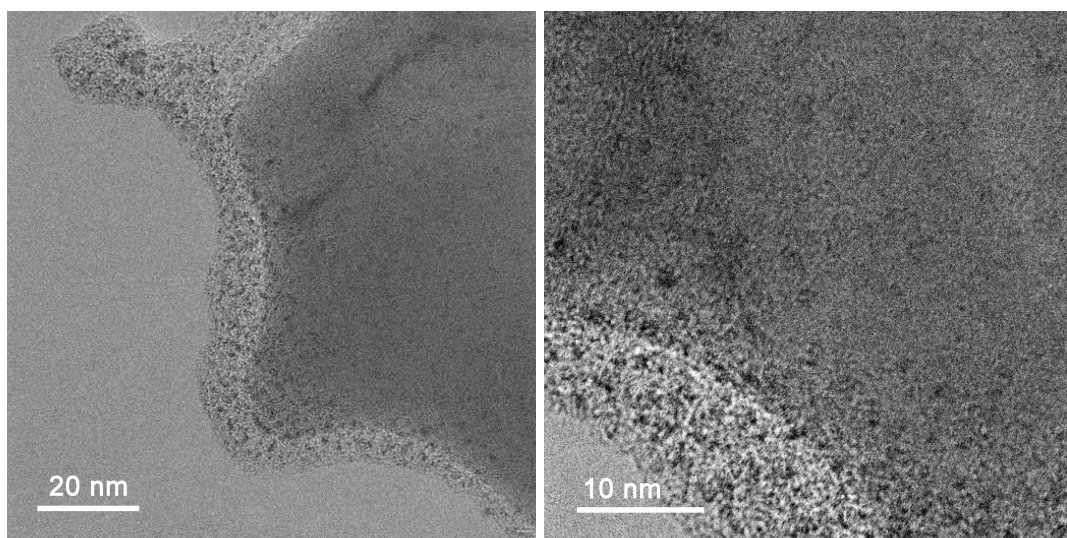
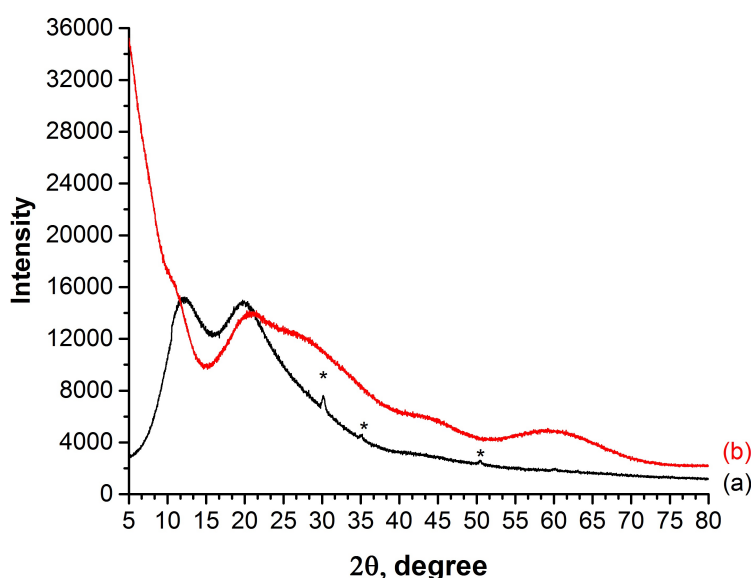
### 2.4. Statistical analysis

The experiments were conducted in 3 – 4 repetitions, with analytical estimations done for each WO<sub>3</sub> NPs concentration in three repetitions. Experimental results were compared with the control. Statistical analysis was performed using the methods of variation statistics. We determined the mean values and the standard deviation of the mean. The significance of differences between the groups was determined by Student t-test. The obtained data were processed using GraphPad 6.0 and Microsoft Excel 2007 software.

## 3. Results and discussion

According to HR-TEM (Fig. 1), WO<sub>3</sub> nanoparticles are ultra small and about 1 nm in size. Obviously, the growth of WO<sub>3</sub> nanoparticles was effectively suppressed by the presence of PVP surfactant.

The XRD data are presented in Fig. 2. The XRD pattern of a dried PVP solution (Fig. 2(a)) contains two broad maxima at 12.1° and 19.9°2 $\theta$  which are characteristic for pure PVP. These data are in a good agreement with previously reported results [14, 15]. The sharp peaks are corresponding to ITO substrate signal. The XRD pattern of the dried WO<sub>3</sub> sol (Fig. 2(b)) is mostly X-ray amorphous and partially similar to PVP XRD pattern. A significant increase in intensity at 2 $\theta$  < 10° may be due to X-ray scattering on ultra small WO<sub>3</sub> nanoparticles.

FIG. 1. HR-TEM image of PVP-stabilized  $WO_3$  nanoparticlesFIG. 2. X-ray diffraction patterns of dried PVP solution (a) and dried  $WO_3$  sol (b). ITO substrate diffraction maxima are marked with \*

The FTIR spectra of dried PVP solution and  $WO_3$  sol are shown in Fig. 3. The spectrum for dried PVP solution is similar to the spectra of individual PVP given in literature [16–18]. The FTIR spectrum of dried  $WO_3$  sol is identical to dried PVP solution excepting the ranges of  $795 - 995 \text{ cm}^{-1}$  and  $420 - 435 \text{ cm}^{-1}$ . Absorbance in these ranges is typical for tungsten oxide [19–22]. Note that FTIR spectrum of dried  $WO_3$  sol after UV irradiation ( $\lambda = 365 \text{ nm}$ , exposure time – 1 min) is similar to dried  $WO_3$  sol kept in dark, while a slight difference in splitting of the absorption band at  $430 \text{ cm}^{-1}$  is observed. Such a difference can be caused by distortions of  $[WO_6]$  octahedra upon changes in tungsten oxidation state.

The appearance of the test tubes with RBCs upon exposure to  $WO_3$  NPs for 2 h is shown in Fig. 4(a). It can be seen that hemolytic activity of  $WO_3$  NPs is dose-dependent. High concentrations of  $WO_3$  NPs lead to the aggregation of the particles, which increases hemolytic activity. It is also well known that tungsten oxide nanoparticles possess enormous redox activity, which can lead to oxidative damage of red blood cell membranes [6].

The results of the spectrophotometric analysis of supernatants confirm the trend revealed by the appearance of the RBCs (Fig. 4(b)). Optical microphotographs of RBCs without  $WO_3$  NPs (Fig. 4(c)) showed cells with

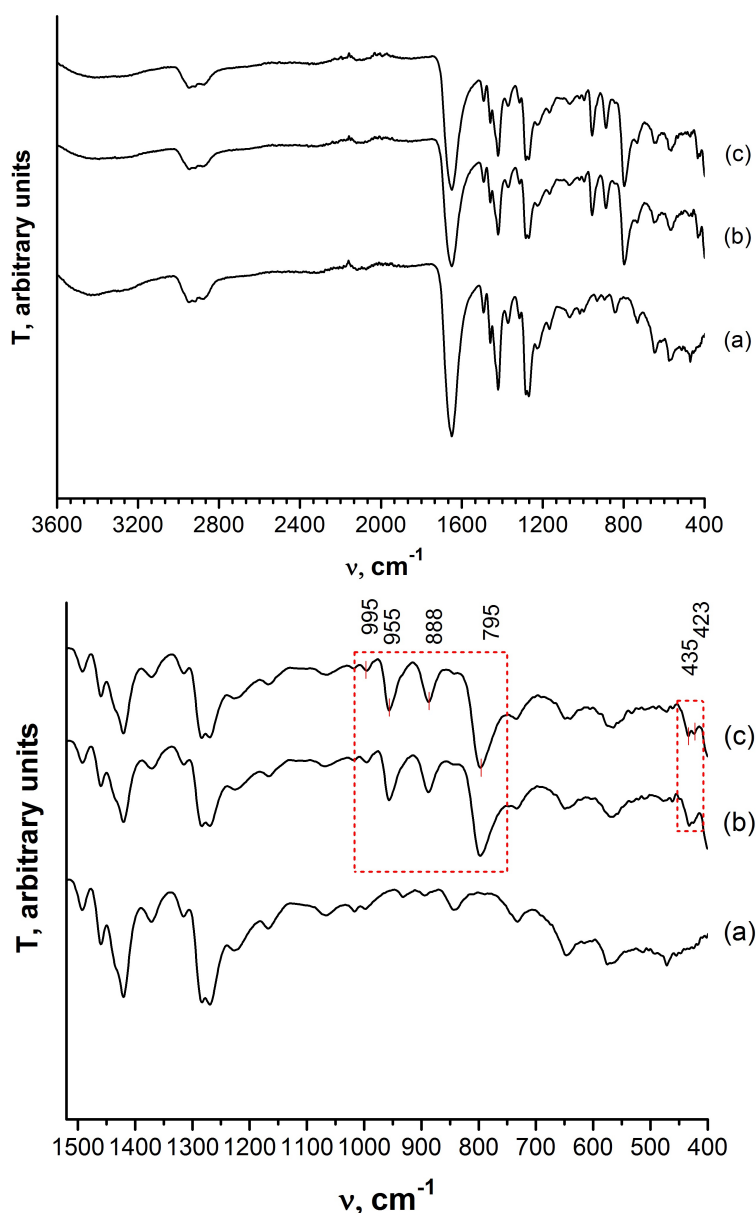


FIG. 3. Survey IR spectrum (above), and its fragment (below): dried PVP solution (a), dried  $\text{WO}_3$  sol (b), dried  $\text{WO}_3$  sol after UV irradiation (c)

undamaged membranes, however treatment with  $\text{WO}_3$  NPs (12.5 mg/ml) for 2 h caused damage to 100 % of RBCs with hemoglobin release and cell lysis leading to formation erythrocyte membrane ghosts (Fig. 4(d)).

Surface functionality of nanoparticles is one of the key factors determining their possible uses in therapeutic applications, imparting functional properties and dictating their circulation profile in the blood stream [23,24]. For example, the nanoparticles' surface hydrophobicity has a critical role in the cellular uptake, toxicity, and immune responses of nanomaterials [25–27]. Meanwhile, when entering the bloodstream, nanoparticles interact with blood proteins to form a protein corona, which changes their functional characteristics thus affecting final physiological effect [28–32]. It was previously shown that the preincubation of nanoparticles with plasma proteins can give rise to hemolytic activity of nanomaterials [33]. In our experiments, we also simulated the conditions of the microenvironment in the bloodstream by preincubating nanoparticles in a solution of serum albumin, the main protein of the blood plasma, and evaluated their hemolytic activity upon this treatment (Fig. 5).

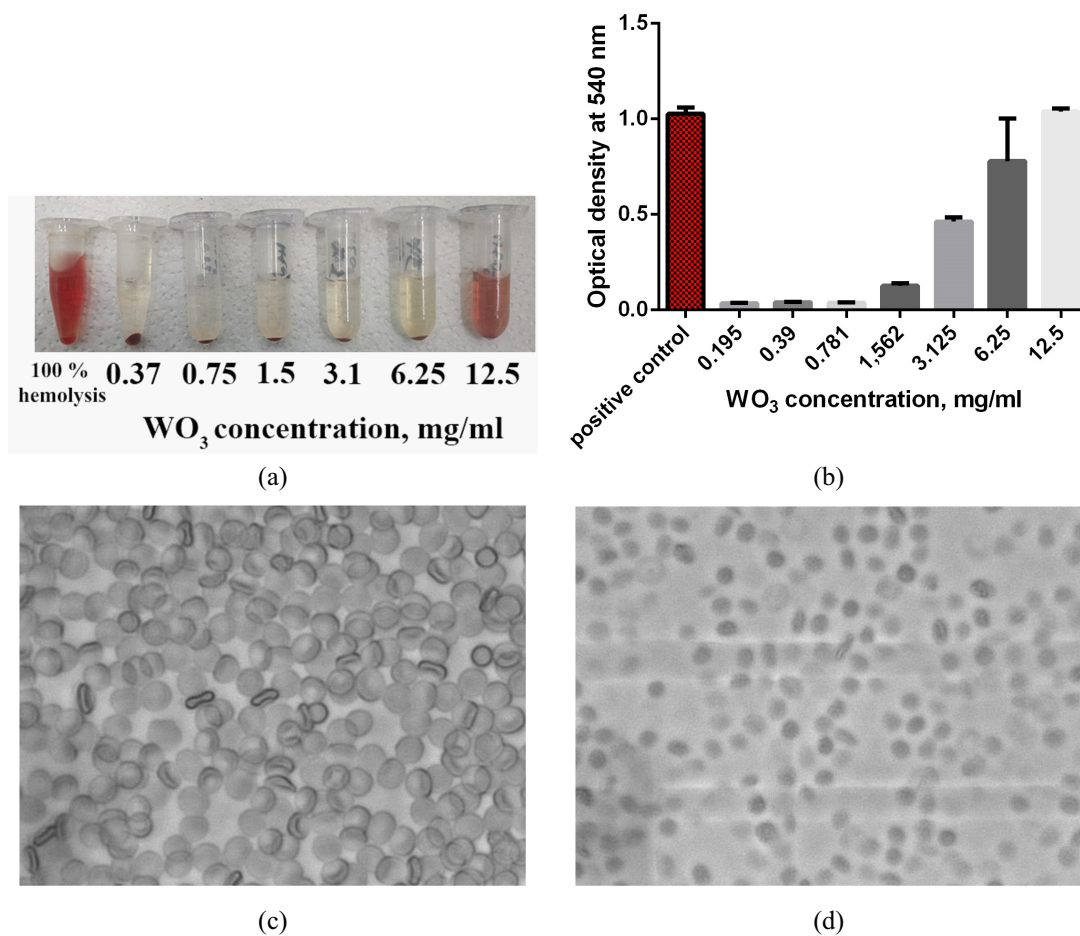


FIG. 4. Hemolysis of human red blood cells upon incubation with  $WO_3$  nanoparticles. Appearance of the test tubes containing RBCs upon exposure to  $WO_3$  NPs for 2 h (a). The hemolysis of  $WO_3$  nanoparticles measured spectrophotometrically at 540 nm (b). Optical microscopy images of RBCs without  $WO_3$  NPs (c) and RBCs exposed to  $WO_3$  NPs (12.5 mg/ml) for 2 h (d)

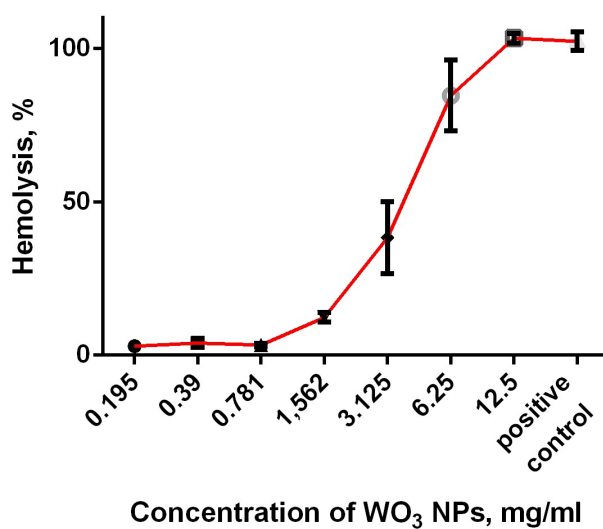


FIG. 5. Hemolytic activity of  $WO_3$  NPs after preincubation with serum albumin. The rate of hemolysis was calculated using water (Milli Q) as the positive control. Error bars represent standard deviations ( $n = 3$ )

Meanwhile, no significant changes in hemolytic activity of WO<sub>3</sub> NPs were observed in the presence of serum albumin.

Thus, the toxic action of tungsten oxide nanoparticles on human blood cells is probably realized via molecular mechanisms. Further research is required to clarify the nature of this toxic action.

#### 4. Conclusions

Ultra small tungsten oxide nanoparticles were synthesized using polyvinylpyrrolidone as the growth regulator. Tungsten oxide nanoparticles were comprehensively studied using HR-TEM, XRD and FTIR techniques.

PVP-stabilized tungsten oxide nanoparticles were shown to exhibit notable hemolytic activity in a dose-dependent manner. The reasons for WO<sub>3</sub> NPs' toxic action were clarified.

#### Acknowledgements

The work supported by Russian Science Foundation (project 18-73-10150).

#### References

- [1] Hosseini F., Rasuli R., Jafarian V. Immobilized WO<sub>3</sub> nano-particles on graphene oxide as a photo-induced antibacterial agent against UV resistant *Bacillus Pumilus*. *J. Phys. D: Appl. Phys.*, 2018, **51** (14), 145403.
- [2] Hariharan V., Radhakrishnan S., et al. Synthesis of polyethylene glycol (PEG) assisted tungsten oxide (WO<sub>3</sub>) nanoparticles for L-dopa bio-sensing applications. *Talanta*, 2011, **85** (4), P. 2166–2174.
- [3] Deng K., Hou Z., et al. Enhanced Antitumor Efficacy by 808 nm Laser-Induced Synergistic Photothermal and Photodynamic Therapy Based on an Indocyanine-Green-Attached W<sub>18</sub>O<sub>49</sub> Nanostructure. *Adv. Funct. Mater.*, 2015, **25** (47), P. 7280–7290.
- [4] Chen Z., Wang Q., et al. Ultrathin PEGylated W<sub>18</sub>O<sub>49</sub> nanowires as a new 980 nm-laser-driven photothermal agent for efficient ablation of cancer cells in vivo. *Adv. Mater.*, 2013, **25** (14), P. 2095–2100.
- [5] Sharker S.Md., Kim S.M., et al. Functionalized biocompatible WO<sub>3</sub> nanoparticles for triggered and targeted in vitro and in vivo photothermal therapy. *J. Control. Release*, 2015, **217**, P. 211–220.
- [6] Zhou Z., Kong B., et al. Tungsten Oxide Nanorods: An Efficient Nanoplatfor for Tumor CT Imaging and Photothermal Therapy. *Sci. Rep.*, 2014, **4**, 3653.
- [7] Liu J., Han J., et al. *In vivo* near-infrared photothermal therapy and computed tomography imaging of cancer cells using novel tungsten-based theranostic probe. *Nanoscale*, 2014, **6** (11), P. 5770–5776.
- [8] Liu P., Wang Y., et al. Ultrasmall WO<sub>3-x</sub>@γ-poly-L-glutamic Acid Nanoparticles as a Photoacoustic Imaging and Effective Photothermal-Enhanced Chemodynamic Therapy Agent for Cancer. *ACS Appl. Mater. Interfaces*, 2018, **10** (45), P. 38833–38844.
- [9] Chen L.Q., Fang L., et al. Nanotoxicity of silver nanoparticles to red blood cells: Size-dependent adsorption, uptake and hemolytic activity. *Chem. Res. Toxicol.*, 2015, **28** (3), P. 501–509.
- [10] Aisaka Y., Kawaguchi R., Watanabe S. Hemolysis Caused by Titanium Dioxide Particles. *Inhalation Toxicol.*, 2008, **20**, P. 891–893.
- [11] Vinardell M.P., Sordé A., et al. Comparative effects of macro-sized aluminum oxide and aluminum oxide nanoparticles on erythrocyte hemolysis: influence of cell source, temperature, and size. *J. Nanopart. Res.*, 2015, **17**, 80.
- [12] Babu E.P., Subastri A., et al. Size Dependent Uptake and Hemolytic Effect of Zinc Oxide Nanoparticles on Erythrocytes and Biomedical Potential of ZnO-Ferulic acid Conjugates. *Sci. Rep.*, 2017, **7**, 4203.
- [13] Dobrovolskaia M.A., Clogston J.D., et al. Method for analysis of nanoparticle hemolytic properties in vitro. *Nano Lett.*, 2018, **8**, P. 2180–2187.
- [14] El Hotaby W., Sherif H.H.A., et al. Assessment of in situ-Prepared Polyvinylpyrrolidone-Silver Nanocomposite for Antimicrobial Applications. *Acta Phys. Pol. A*, 2017, **131** (6), P. 1554–1560.
- [15] Li X.G., Kresse I., et al. Morphology and gas permselectivity of blend membranes of polyvinylpyridine with ethylcellulose. *Polymer*, 2001, **42** (16), P. 6859–6869.
- [16] Liu H., Zhang B., et al. Hydrothermal synthesis of monodisperse Ag<sub>2</sub>Se nanoparticles in the presence of PVP and KI and their application as oligonucleotide labels. *J. Mater. Chem.*, 2008, **18** (22), P. 2573–2580.
- [17] Melnikova O.A., Samkova I.A., Melnikov M.Yu., Petrov A.Yu. IR-spektroskopische studies of chemical structure of polymeric complexes of medicinal substances on the basis of polyvinylpyrrolidone. *Advances in current natural sciences*, 2016, **8**, P. 42–49.
- [18] Basha M.A.F. Magnetic and optical studies on polyvinylpyrrolidone thin films doped with rare earth metal salts. *Polym. J.*, 2010, **42**, P. 728–734.
- [19] Balzer R., Drago V., Schreiner W.H., Probst L.F.D. Synthesis and Structure-Activity Relationship of a WO<sub>3</sub> Catalyst for the Total Oxidation of BTX. *J. Braz. Chem. Soc.*, 2014, **25** (11), P. 2026–2031.
- [20] Prabhu N., Agilan S., et al. Effect of temperature on the structural and optical properties of WO<sub>3</sub> nanoparticles prepared by solvo thermal method. *Digest Journal of Nanomaterials and Biostructures*, 2013, **8** (4), P. 1483–1493.
- [21] Kumar V.B., Mohanta D. Formation of nanoscale tungsten oxide structures and colouration characteristics. *Bull. Mater. Sci.*, 2011, **34** (3), P. 435–442.
- [22] He G.H., Liang C.J., et al. Preparation of novel Sb<sub>2</sub>O<sub>3</sub>/WO<sub>3</sub> photocatalysts and their activities under visible light irradiation. *Mater. Res. Bull.*, 2013, **48** (6), P. 2244–2249.
- [23] Saha K., Bajaj A., Duncan B., Rotello V.M. Beauty is skin deep: a surface monolayer perspective on nanoparticle interactions with cells and bio-macromolecules. *Small*, 2011, **7**, P. 1903–1918.
- [24] Mout R., Moyano D.F., Rana S., Rotello V.M. Surface functionalization of nanoparticles for nanomedicine. *Chem. Soc. Rev.*, 2012, **41**, P. 2539–2544.

- [25] Zhu Z.J., Posati T., et al. The Interplay of Monolayer Structure and Serum Protein Interactions on the Cellular Uptake of Gold Nanoparticles. *Small*, 2012, **8**, P. 2659–2663.
- [26] Chompoosor A., Saha K., et al. The role of surface functionality on acute cytotoxicity, ROS generation and DNA damage by cationic gold nanoparticles. *Small*, 2010, **6**, P. 2246–2249.
- [27] Moyano D.F., Goldsmith M., et al. Nanoparticle Hydrophobicity Dictates Immune Response. *J. Am. Chem. Soc.*, 2012, **134**, P. 3965–3967.
- [28] Walkey C.D., Chan W.C.W. Understanding and controlling the interaction of nanomaterials with proteins in a physiological environment. *Chem. Soc. Rev.*, 2012, **41**, P. 2780–2799.
- [29] Monopoli M.P., Aberg C., Salvati A., Dawson K.A. Biomolecular coronas provide the biological identity of nanosized materials. *Nat. Nanotechnol.*, 2012, **7**, P. 779–786.
- [30] Arvizo R.R., Giri K., et al. Identifying New Therapeutic Targets via Modulation of Protein Corona Formation by Engineered Nanoparticles. *PLoS One*, 2012, **7**, e33650.
- [31] Salvador-Morales C., Flahaut E., et al. Complement activation and protein adsorption by carbon nanotubes. *Mol. Immunol.*, 2006, **43**, P. 193–201.
- [32] Owens D.E., Peppas N.A. Opsonization, biodistribution, and pharmacokinetics of polymeric nanoparticles. *Int. J. Pharm.*, 2006, **307**, P. 93–102.
- [33] Saha K., Moyano D.F., Rotello V.M. Protein coronas suppress the hemolytic activity of hydrophilic and hydrophobic nanoparticles. *Mater Horiz.*, 2014, **1**, P. 102–105.